J|A|C|S
ARTICLES
Published on Web 12/20/2006

Organometallics Meet Colloid Chemistry: A Case Study in Three Phases Based on Molecular Carbonyl Precursors Containing Zinc and Manganese

A. Orlov,[†,§] A. Roy,[‡] M. Lehmann,[†] M. Driess,[†] and S. Polarz*[,†,§]

Contribution from the Technical University Berlin, Strasse des 17. Juni 135, 10623 Berlin, Germany, and University of Duisburg-Essen, 47057 Duisburg, Germany

Received August 16, 2006; E-mail: sebastian.polarz@tu-berlin.de

Abstract: Two organometallic compounds containing zinc and manganese in different ratios are used as single-source precursors for the preparation of various new, bimetallic oxide materials with nanoscaled dimensions. It is shown that the materials synthesis can be performed in the solid-state, the liquid-phase, and even in the gas-phase. The molecular composition of the precursors determines the composition of the resulting materials. In addition, two novel methods for the preparation of highly crystalline metal oxide colloids are presented: The coupling between a gas-phase process and a colloidal approach, and the application of ozone as an oxidant for the transformation of metal carbonyls into oxides in the liquid phase.

Introduction

Nanoparticles,[1] in particular those of semiconducting metal chalkogenides, have received steadily growing attention due to their high potential for nanotechnological devices. Higher complexity and a wider range of properties emerge for materials containing not only one but at least two metals.[2,3] Impressive examples for functional heterobimetallic chalkogenides are materials exhibiting the so-called giant magnetoresistance effect.[4] A new research field has emerged commonly known as "spintronics."[5] Currently, diluted magnetic semiconductors are considered as the most promising candidates for spintronics.[6] Among those, zinc oxide doped with Mn^{2+} currently receives major attention.[7,8] However, it is worth noting that the Zn/Mn/O system offers two more functional materials: $ZnMn_2O_4$ with Spinel structure, and $ZnMnO_3$ (Ilmenite structure). Various applications have been reported for the latter materials, ranging from catalysis,[9] as electrode materials for advanced batteries,[10] as sensors, as anticorrosive coatings, to magnetic applications.[8]

Three factors mainly influence the (functional) properties of semiconducting, bimetallic oxides: The degree of dispersion of the two metals in the oxide matrix, the primary size of the particles, and the aggregation state of those particles. The degree of dispersion of the metals in the oxide should be at maximum. Phase separation or clustering if undesired needs to be avoided. The mentioned, ideal dispersion can be very hard to obtain in case two separate metal sources are used because different precursors are likely to possess different chemical and physical properties (e.g., reactivity, solubility, etc.). Consequently, it is challenging to "predetermine" materials on the molecular scale with regard to composition. Such compounds are known as single-source precursors.[11] They bear the potential that throughout the entire process of materials synthesis the relevant elements remain dispersed in molecular fashion.

In the current manuscript, innovative, heterobimetallic precursors for the generation of $Zn_xMn_yO_z$ materials are described. It is demonstrated how the composition of the materials can be

† Technical University Berlin.
‡ University of Duisburg-Essen.
§ Present address: University Konstanz, 78457 Konstanz, Germany.

(1) Fendler, J. H.; Meldrum, F. C. *Adv. Mater.* **1995**, *7* (7), 607−632; Rao, C. N. R.; Kulkarni, G. U.; Thomas, P. J.; Edwards, P. P. *Chem. Soc. Rev.* **2000**, *29* (1), 27−35.
(2) Toshima, N.; Yonezawa, T. *New J. Chem.* **1998**, *22* (11), 1179−1201.
(3) Niederberger, M.; Pinna, N.; Polleux, J.; Antonietti, A. *Angew. Chem., Int. Ed.* **2004**, *43* (17), 2270−2273; Niederberger, M.; Garnweitner, G.; Pinna, N.; Antonietti, M. *J. Am. Chem. Soc.* **2004**, *126* (29), 9120−9126.
(4) Dagotto, E.; Hotta, T.; Moreo, A. *Phys. Rep.-Rev. Sec. Phys. Lett.* **2001**, *344* (1−3), 1−153.
(5) Zutic, I.; Fabian, J.; Das Sarma, S. *Rev. Mod. Phys.* **2004**, *76* (2), 323−410; Wolf, S. A.; Awschalom, D. D.; Buhrman, R. A.; Daughton, J. M.; von Molnar, S.; Roukes, M. L.; Chtchelkanova, A. Y.; Treger, D. M., *Science* **2001**, *294* (5546), 1488−1495; Ohno, H. *Science* **1998**, *281* (5379), 951−956; Ball, P. *Nature* **2000**, *404*, 918−920.
(6) Dietl, T.; Ohno, H.; Matsukura, F.; Cibert, J.; Ferrand, D. *Science* **2000**, *287* (5455), 1019−1022; Ohno, Y.; Young, D. K.; Beschoten, B.; Matsukura, F.; Ohno, H.; Awschalom, D. D. *Nature* **1999**, *402* (6763), 790−792.
(7) Kolesnik, S.; Dabrowski, B.; Mais, J. *J. Appl. Phys* **2004**, *95* (5), 2582−2586; Coey, J. M. D.; Viret, M.; von Molnar, S. *Adv. Phys.* **1999**, *48* (2), 167−293; Luo, J.; Liang, J. K.; Liu, Q. L.; Liu, F. S.; Zhang, Y.; Sun, B. J.; Rao, G. H. *J. Appl. Phys.* **2005**, *97* (8), Art No. 086106; Garcia, M. A.; Ruiz-Gonzalez, M. L.; Quesada, A.; Costa-Kramer, J. L.; Fernandez, J. F.; Khatib, S. J.; Wennberg, A.; Caballero, A. C.; Martin-Gonzalez, M. S.; Villegas, M.; Briones, F.; Gonzalez-Calbet, J. M.; Hernando, A. *Phys. Rev. Lett.* **2005**, *94* (21), Art. No. 217206.
(8) Mofor, A. C.; El-Shaer, A.; Bakin, A.; Wehmann, H. H.; Ahlers, H.; Siegner, U.; Sievers, S.; Albrecht, M.; Schoch, W.; Izyumskaya, N.; Avrutin, V.; Stoemenos, J.; Waag, A. *Superlattices Microstruct.* **2006**, *39* (1−4), 381−386.
(9) Bessekhouad, Y.; Robert, D.; Weber, J. V. *Catal. Today* **2005**, *101* (3−4), 315−321.
(10) Yang, H.; Yang, H. Q.; Lu, Y. L.; Li, N.; Li, B. X. *J. Power Sources* **1996**, *62* (2), 223−227; Guillernet-Fritsch, S.; Chanel, C.; Sarrias, J.; Bayonne, S.; Rousset, A.; Alcobe, X.; Martinez Sarrion, M. L. *Solid State Ionics* **2000**, *128* (1−4), 233−242.
(11) Mathur, S.; Veith, M.; Shen, H.; Hufner, S., Single-step preparation of nanocomposites. In *Metastable, Mechanically Alloyed And Nanocrystalline Materials*; Trans Tech Publications: Zurich, 2002; Vols. 386−3, pp 341−346; Veith, M.; Altherr, A.; Lecerf, N.; Mathur, S.; Valtchev, K.; Fritscher, E. *Nanostruct. Mater.* **1999**, *12* (1−4), 191−194; Veith, M.; Mathur, S.; Mathur, C. *Polyhedron* **1998**, *17* (5−6), 1005−1034; Herron, N.; Thorn, D. L. *Adv. Mater.* **1998**, *10* (15), 1173−1184.

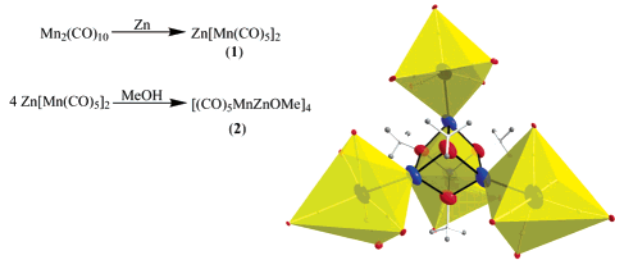

Figure 1. Synthetic steps leading to the molecular precursors used in this study and the structure of **2** determined by single-crystal X-ray analysis presented here for the first time (red ≅ O; blue ≅ Zn; black ≅ Mn; light gray ≅ C; gray ≅ H). The 'Zn_4O_4' heterocubane core and the distorted '$(CO)_5Mn-Zn$' octahedrons are highlighted in green.

encoded on the molecular scale. Furthermore, new methods to obtain the materials in nanocrystalline and in colloidal form are presented.

Results and Discussion

The Precursors. The synthesis strategy for the desired precursors containing zinc, manganese, and oxygen is inspired by the simple reaction of elemental zinc with halogens ($Zn + X_2 \rightarrow ZnX_2$). Previous investigations show that the $Mn(CO)_5$ fragment can be characterized as a pseudohalogen.[12] Consequently, $Mn_2(CO)_{10}$ reacts readily with elemental zinc under insertion of one zinc atom into the Mn−Mn bond in $Mn_2(CO)_{10}$ and furnishes $Zn[Mn(CO)_5]_2$ (**1**). Then, in analogy to the zinc dihalogenides (ZnX_2), **1** can undergo ligand exchange reactions. Methanolysis of **1** affords the volatile $HMn(CO)_5$ (≈HX elimination) and the tetrameric zinc methoxide cluster (**2**; Figure 1). **2** contains a "Zn_4O_4" core with four terminal $Mn(CO)_5$ groups σ-bonded to the Zn atoms (Figure 1). Obviously, both organometallic compounds (**1** and **2**) fulfill the requirement to contain the required elements for the formation of $Zn_xMn_yO_z$ materials. The precursors differ regarding the ratio of Zn:Mn.

Preparation of Nanopowders. The simplest way to transform the mentioned precursors into the respective oxides is their decomposition in the solid state in the presence of oxygen. Products were initially analyzed by powder X-ray diffractometry (PXRD) presented in Figure 2a. It is seen that the ratio of zinc to mangenese in the precursors determines which oxide is formed. $Zn[Mn(CO)_5]_2$ affords $ZnMn_2O_4$ (Zn:Mn ratio 1:2), the heterobimetallic cubane **2** furnishes $ZnMnO_3$ (Zn:Mn ratio 1:1). The formation of $ZnMnO_3$ is furthermore interesting because it was reported that this phase can be obtained by classical solid-state synthesis methods only at high pressures (65 kbar).[13] In both cases, nanocrystalline oxides are obtained. Particle sizes were calculated by evaluating the width of the reflexes using the Scherrer equation. For $ZnMn_2O_4$ an average particle size of $D_p = 8.4$ nm was obtained. The particles of $ZnMnO_3$ are significantly smaller ($D_p = 5.13$ nm). However, it is seen from transmission electron microscopy (TEM; Figure 2b for $ZnMnO_3$; see Supporting Information (SI) for $ZnMn_2O_4$) that the primary particles form large agglomerates. EDX measurements performed on the agglomerates support the PXRD results: Phases with Zn:Mn ratios of ≈1:1 (Figure 2c) (and 1:2 from

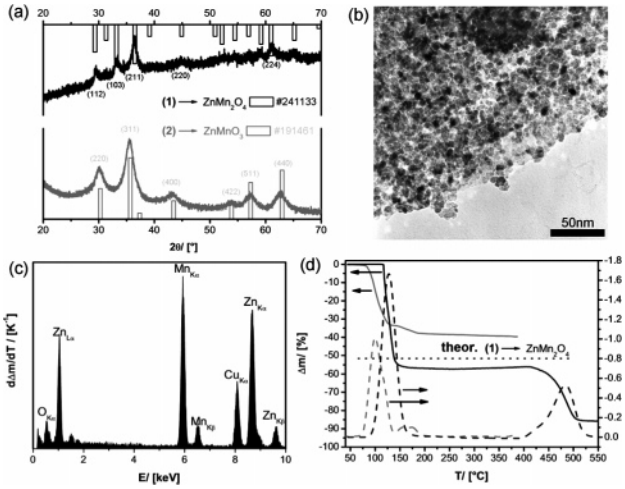

Figure 2. PXRD patterns (a) for the oxidative transformation of precursors **1** (black; prepared at 550 °C) and **2** (gray; prepared at 300 °C) to the respective oxides, and the reference patterns for $ZnMnO_3$ and $ZnMn_2O_4$. (b) TEM image of the obtained $ZnMnO_3$ nanopowder and the EDX spectrum (c). The signals for copper in the EDX spectrum originate from TEM grid used for the measurement. TGA traces (d).

$Zn[Mn(CO)_5]_2$; see Supporting Information) could be obtained. For obtaining more information about the transformation process (from the molecule to the material), the decomposition was monitored by thermogravimetric analysis (TGA) shown in Figure 2d. An analysis of the oxidation states ($[(CO)_5Mn^{-I}]_2Zn^{II} \rightarrow Zn^{II}Mn^{III}{}_2O_4$ and $[(CO)_5Mn^{-I}Zn^{II}OCH_3]_4 \rightarrow Zn^{II}Mn^{III}O_3$) indicates that the transformation process concerns mainly the oxidation of the formally, monoanionic $[(CO)_5Mn]^-$ fragment.

For precursor **2** one finds one major mass-loss step with a decomposition maximum at $T = 100$ °C followed by two less significant steps. Already at 200 °C the "transformation" of the precursor is finished. At this temperature however, one finds only an amorphous phase which crystallizes at a temperature of ≥300 °C (Figure 2a). If one compares to precursor **1**, it is interesting to note that the experimentally determined mass loss ($\Delta m_{exp} = -86.2\%$) is much larger than theoretically expected for the transformation **1** → $ZnMn_2O_4$ ($\Delta m_{theor} = -52.1\%$; see Figure 2). The significant mass loss at 128 °C can be attributed to the evaporation of the pure precursor. Compound **1** possesses significant volatility which fits to the observation that the purification of **1** involves sublimation (see Experimental Section) and that after the reaction the entire TGA vessel was contaminated with $ZnMn_2O_4$. The transformation of the oxide becomes complete for temperatures above 550 °C.

The volatility of **1** allows preparation of $ZnMn_2O_4$ not only in the solid state but also in the gas phase. First, the $Zn[Mn(CO)_5]_2$ is evaporated under inert-gas conditions, and oxygen is added to the precursor aerosol which is then led into a second oven (for a more detailed description see the Supporting Information). The described process is known as chemical vapor synthesis (CVS) and has been used by us for the formation of various nanoscaled oxide materials recently.[14,15] Due to the high dilution of the precursor in the aerosol, its is possible to apply rather high temperatures while less aggregated, and still very small particles can be obtained (Figure 3b). The

(12) Burlitch, J. M.; Hayes, S. E.; Whitwell, G. E., II. *Organometallics* **1982**, *1*, 1074−1083.
(13) Chamberland, B. L.; Sleight, A. W.; Weiher, J. F. *J. Solid-State Chem.* **1970**, *1*, 512−514.
(14) Polarz, S.; Roy, A.; Merz, M.; Halm, S.; Schröder, D.; Scheider, L.; Bacher, G.; Kruis, F. E.; Driess, M. *Small* **2004**, *1*, 540−552.
(15) Roy, A.; Polarz, S.; Rabe, S.; Rellinghaus, B.; Zahres, H.; Kruis, F. E.; Driess, M. *Chem. Eur. J.* **2004**, *10* (6), 1565−1575.

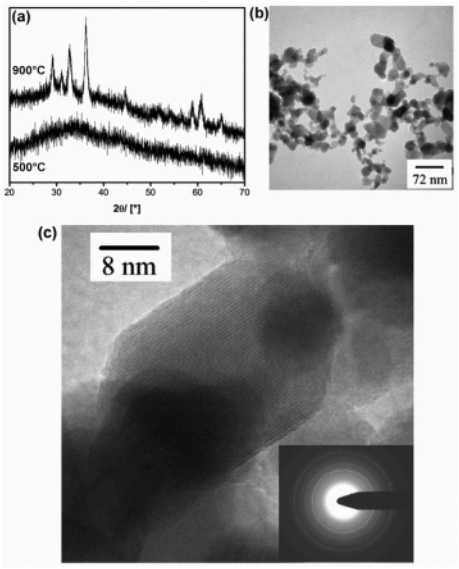

Figure 3. Samples prepared by CVS: (a) PXRD patterns of samples prepared at two different temperatures; TEM (b, c) of the sample prepared at 900 °C.

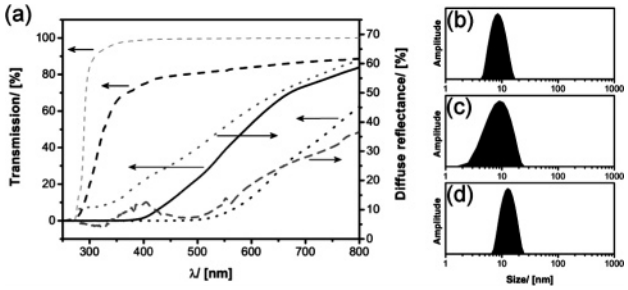

Figure 4. (a) UV−vis data of the $ZnMn_2O_4$ (gray dashed) and $ZnMnO_3$ (gray dotted) nanopowders measured in diffuse reflectance mode, and of colloidal solutions of $ZnMn_2O_4$ from CVS (black dashed) and from the colloidal route (black solid) and of $ZnMnO_3$ (black dotted) measured in transmission mode in comparison to the cuvette as a reference (light gray dashed). Particle size distribution curves from dynamic light scattering measurements (DLS): (b) $ZnMn_2O_4$ colloids from the CVS route; $ZnMn_2O_4$ (c) and $ZnMnO_3$ (d) colloids prepared via the colloidal route.

particles are highly crystalline as indicated by the lattice fringes seen in high-resolution TEM (HRTEM) images (Figure 3c). In comparison to the aforementioned process in the solid state, the crystallization of $ZnMn_2O_4$ requires similarly high temperatures. A sample prepared at 500 °C is practically amorphous while for 900 °C 15 nm large particles can be obtained (Figure 3a).

Preparation of Colloids. The materials described so far were powders with different aggregation degrees of the primary particles. It would be of advantage if it became possible to manipulate the single oxide nanocrystals further. Therefore, our next aim was to transform the nanopowders into colloidal solutions.[3]

The first attempt was to redisperse nanoparticles originating from the solid-state process (Figure 2b). The nanopowders were dispersed in THF and were ultrasonificated in the presence of different surfactants (anionic, cationic, and nonionic). The dispersions were filtered through a filter with 250 nm pore width. The resulting, clear solutions were analyzed using UV/vis spectroscopy. Because both oxides, $ZnMn_2O_4$ and $ZnMnO_3$, are brown (Figure 4a), it can be expected that colloidal solution will be brown as well. Unfortunately, no absorption was detected, indicating that the redispersion of the nanocrystalline oxide powders was not successful. Apparently, the particles of the powders prepared by the solid-state route are aggregated too strongly.

Because the aggregation state of the CVS materials (Figure 3b) is much lower, combining the gas-phase preparation process with colloid chemistry could potentially be very promising. To the best of our knowledge this approach is a unique, yet unprecedented method to gain access to metal-oxide colloids. Instead of depositing the oxide aerosol on a solid substrate, the aerosol was bubbled through a THF solution containing amphiphiles (see Supporting Information). After filtration, a light brown, clear solution was obtained as confirmed by UV/vis spectroscopy (Figure 4a). Dynamic light scattering performed on the filtered solutions showed that colloids with an average hydrodynamic radius of 4.2 nm have been obtained. TEM and PXRD measurements support this conclusion (see Supporting Information paragraph). The advantage of the new approach to prepare colloids involving a gas-phase step in comparison to more traditional methods is that it is now possible to adjust the particle size of the crystalline inorganic phase in a continuous manner because the particle size can be controlled by changing the synthesis temperature applied to the aerosol.[14] On the other hand, the approach has some disadvantages as well. The yield for the transformation of the aerosol into a colloidal solution is relatively low (max. 15%), and one is limited to volatile precursor compounds. Precursor **2** cannot be used in this process due to its low decomposition temperature (Figure 2).

However, both precursor compounds (**1** and **2**) are soluble in organic solvents. Therefore, one may also consider more classical routes to obtain colloids. There is one problem: The oxidative process necessary for the formation of the materials cannot be performed analogously to the methods described for the solid state or for the gas phase. Simple heating of the precursors in a high-boiling point solvent like diphenylether leads to undefined products and probably to a separation of Zn and Mn. The problem is obviously that in solution dissolved oxygen is not powerful enough to oxidize the precursors. In particular by using IR spectroscopy it was found that it is very hard to remove the CO groups from the precursors. Therefore, ozone instead of oxygen was selected as a stronger oxidation agent. Like the latter, it also does not introduce any additional, undesired chemical elements as contamination. $CHCl_3$ was used as a solvent because it is known to be resistant toward ozone. During bubbling a mixture of ozone and oxygen through a solution of the precursors containing cetyltrimethylammonium bromide (CTAB) as a surfactant, the solutions turned rapidly from slightly yellow to dark brown (see Supporting Information). Subsequently, the solvent was removed by evaporation and PXRD and FT-IR were recorded from the obtained dry powders. It becomes evident that due to the treatment with ozone, both precursors **1** and **2** have been quantitatively reacted. The CO bands at ($\tilde{\nu} \approx 2000$ cm^{-1}) have disappeared in the products (Figure 5 c → d; f → g). The "colloidal powders" are characterized by a superposition of the spectrum of CTAB (Figure 5b) and the respective oxides $ZnMn_2O_4$ (Figure 5 a ← d; characteristic band at 504 and 613 cm^{-1}) or $ZnMnO_3$ (Figure 5 e ← g; characteristic band at 512 and 613 cm^{-1}). The PXRD patterns of the colloidal powders (Figure 5h and 5j) show no reflections, indicating that the oxide phases are still amorphous at this stage. Therefore, the colloids were redispersed in toluene,

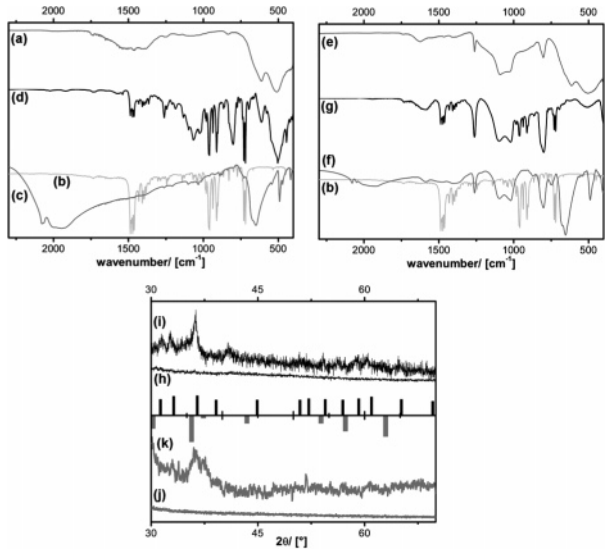

Figure 5. FT-IR spectra of the $ZnMn_2O_4$ nanopowder (a), CTAB (b), $Zn[Mn(CO)_5]$ **1** (c), the $ZnMn_2O_4$ colloids (d), and of the $ZnMnO_3$ nanopowder (e), $[(CO)_5MnZnOCH_3]$ **2** (f), and the $ZnMnO_3$ colloids (g). PXRD patterns of the $ZnMn_2O_4$ colloids prior to the crystallization step (h) and afterward (j). The same is shown for the $ZnMnO_3$ colloids (j, k). The reference reflections are shown as well.

refluxed, and filtered. Clear brown solutions (see UV−vis spectra; Figure 4) were obtained from which DLS, high-resolution TEM (HRTEM) data, and PXRD patterns were acquired. Considering the absolute value of UV/vis transmission shows that the amount of colloids is much larger compared to the CVS route described before. According to particle-size distributions obtained from DLS data (Figure 4c,d), colloids with an average size of 9.2 nm (for $ZnMn_2O_4$) and 12.4 nm (for $ZnMnO_3$) could be obtained. The colloidal solutions were stable. Even after several weeks at RT, no agglomeration occurs.

The particle size determined from DLS measurements is slightly larger compared to the particle size from TEM (Figure 6; $D_p \approx 6$ nm for $ZnMn_2O_4$; $D_p \approx 10$ nm for $ZnMnO_3$). If one takes into account that the particle corona is a solvent-swollen surfactant shell and one considers the size of CTAB, the difference of ≈2−3 nm is quite reasonable because DLS is sensitive to the hydrodynamic radius and not toward the crystalline core of the particles. Remarkably, the redispersion step in toluene has induced crystallization of the particles at very low temperatures compared to the solid-state and gas-phase methods. Isolated particles and lattice fringes can clearly be identified by HRTEM. The evaluation of the lattice parameters found by TEM (see Supporting Information) confirms that the particles contain $ZnMn_2O_4$ (Figure 6a) and $ZnMnO_3$ (Figure 6b), respectively. This conclusion is furthermore supported by PXRD data shown in Figure 5 recorded from solvent-removed powders. After the crystallization step, broad diffraction patterns for the expected oxide phases have appeared. The evaluation of the width of the reflexes is aggravated by the significant noise and is therefore connected to a large error. However, evaluation using the Scherrer equation gives $D_p = 6(\pm 2)$ nm for $ZnMn_2O_4$ and $D_p = 8.4(\pm 2)$ nm for $ZnMnO_3$ which is in good agreement with the TEM data. Obviously, the colloids represent the surfactant-stabilized primary particles.

Conclusion

The first single-source precursors for defined, bimetallic Zn/Mn-oxides were introduced. Nanopowders of the materials

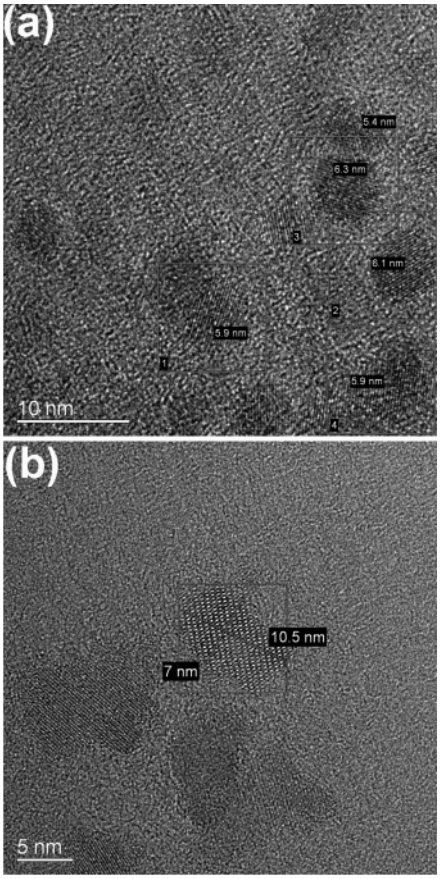

Figure 6. HRTEM micrographs of the $ZnMn_2O_4$ colloids (a) and the $ZnMnO_3$ colloids (b). (Enlargements are shown in the Supporting Information).

$ZnMn_2O_4$ and $ZnMnO_3$ were prepared. It was shown that the composition encoded on the molecular scale determines which oxide is formed. Two novel approaches for the preparation of inorganic colloids were presented, the first one involving the formation of inorganic oxide nanoparticles in the gas phase coupled to a colloid method. In addition, experiments were performed to prepare colloids starting from solutions of the precursors in an organic solvent. It was shown that unlike dioxygen, ozone is very well suited to transform the organometallic carbonyl precursors into the respective oxides. Overall, our results document a unique case for the preparation of functional, nanoscaled materials in not less than three phases: In the solid state, in the gas phase, and in organic solvents.

Experimental Section

Preparation of Compounds. All starting compounds were received from Aldrich and were intensively dried and purified prior to use. The precursors were prepared according to the literature.[12]

$ZnMn_2O_4$ Colloids from the Gas Phase (see also Supporting Information). $Zn[Mn(CO)_5]_2$ (43 mg) was transferred to a tube furnace and was heated at 250 °C under a constant flow of dry N_2. O_2 (50% by volume) was added to the precursor aerosol and led into a second furnace. The decomposition was performed at 620 °C. At the end of the second furnace the oxide aersol was bubbled through a solution of 1.5 g of CTAB in 100 mL of THF.

Oxide Colloids in Organic Solvents. $Zn[Mn(CO)_5]_2$ (28 mg) was dissolved in 20 mL of a 0.05 M solution of CTAB in $CHCl_3$. A mixture of O_3 and O_2 with 200 mg/h of ozone was bubbled through the solution at RT until no further change of the color could be observed. The $CHCl_3$

was removed, and the remaining solid was dispersed in 15 mL of toluene. The resulting dispersion was refluxed for 6 h. The $ZnMnO_3$ colloids were prepared in an analogous way, with the difference being that 12 mg $[CH_3OZnMn(CO)_5]_4$ was used.

Analytical Methods. Dynamic light scattering was measured on a Viscotek 802 DLS instrument with 50 mW diode laser with wavelength 827.9 nm in different solvents. Curves of particle distributions from the intensity of a beam were calculated with the program DynaLS 2.7.1. PXRD analyses of all powder samples were performed on a Siemens D5000 X-ray diffractometer using Cu K_α radiation ($\lambda = 1.5418$ Å). FT-IR spectra were recorded by using a Bruker Vector 22 spectrometer from KBr pellets. UV/vis spectra of both reflection and transmission were recorded by using a Perkin-Elmer Lambda 20 spectrometer equipped with a reflecting sphere Labsphere RSA-PE-20. Thermogravimetric analysis was performed by an instrument from Rubotherm equipped with a magnetic balance system. Conventional transmission electron microscopy (CTEM) was performed on a Philips CM12 microscope (LaB_6 filament, 120 kV, Twin lens) equipped with an energy dispersive X-ray spectrometer (EDX, type Oxford Link). The HRTEM images were recorded at the FEI Tecnai F20/Cs-corr TEM located at the Triebenberg Lab of the TU Dresden. This microscope is equipped with a field emission electron source and operates at 200 kV acceleration voltage. The spherical aberration of the objective lens is corrected by means of a Cs corrector, which allows the correction of all coherent aberrations up to third order. As a consequence, surfaces of clusters are imaged without delocalization showing the true positions of atomic columns. The TEM samples were prepared by shortly dipping a carrier covered with a perforated carbon foil (Plano company, S147) in the solution where the $ZnMnO_3$ particles were dissolved in acetone.

Acknowledgment. We thank Deutsche Forschungsgemeinschaft (Emmy-Noether scholarship, SPP 1119) for financial support. The possibility and support for using the spherical aberration corrected FEI Tecnai F20 TEM in the workgroup of Prof. Hannes Lichte at the Triebenberg Lab of the TU Dresden is gratefully acknowledged. Dr. K. Merz is acknowledged for his support regarding single-crystal analysis.

Supporting Information Available: TEM and EDX of the $ZnMn_2O_4$ nanopowder prepared in the solid-state (SI -1). Setup for the CVS approach (SI -2). TEM and PRXD for the colloids prepared by the CVS method (SI -3). Photographic images of the ozonization reaction (SI -4). FT-evaluation of the HRTEM data (SI-5, SI-6). Enlargements of the HRTEM data (SI-7). CIF file for the X-ray structure of compound **2** (SI-8). This material is available free of charge via the Internet at http://pubs.acs.org.

JA0659626